INSTITUTE OF PLASMA PHYSICS

NAGOYA UNIVERSITY

IMPROVED CONFINEMENT REGIMES IN JIPP T-IIU

T. WATARI, R. KUMAZAWA, K. TOI, Y. HAMADA, A. ANDO, Y. OKA, O. KANEKO, K. KAWAHATA, K. ADATI, R. AKIYAMA, R. ANDO, T. AOKI, J. FUJITA, S. HIDEKUMA, S. HIROKURA, K. IDA, H. IKEGAMI, K. KADOTA, E. KAKO, A. KARITA, Y. KAWASUMI, S. KITAGAWA, M. KOJIMA, T. KAWAMOTO, T. KURODA, K. MASAI, A. MOHRI, S. MORITA, K. NARIHARA, Y. OGAWA, K. OHKUBO, S. OKAJIMA, T. OZAKI, A. SAGARA, M. SAKAMOTO, M. SASAO, K. SATO, K.N. SATO, T. SATO, T. SEKI, F. SHIMBO, H. TAKAHASHI, S. TANAHASHI, Y. TANIGUCHI, T. TSUZUKI

(Received --- Apr. 8, 1989)

IPPJ- 909 Apr. 1989

RESEARCH REPORT

NAGOYA, JAPAN

IMPROVED CONFINEMENT REGIMES IN JIPP T-IIU

T. WATARI, R. KUMAZAWA, K. TOI, Y. HAMADA, A. ANDO,
Y. OKA, O. KANEKO, K. KAWAHATA, K. ADATI, R. AKIYAMA,
R. ANDO, T. AOKI, J. FUJITA, S. HIDEKUMA, S. HIROKURA,
K. IDA, H. IKEGAMI, K. KADOTA, E. KAKO, A. KARITA, Y. KAWASUMI,
S. KITAGAWA, M. KOJIMA, T. KAWAMOTO, T. KURODA, K. MASAI,
A. MOHRI, S. MORITA, K. NARIHARA, Y. OGAWA, K. OHKUBO,
S. OKAJIMA*, T. OZAKI, A. SAGARA, M. SAKAMOTO, M. SASAO, K. SATO,
K.N. SATO, T. SATO, T. SEKI, F. SHIMBO, H. TAKAHASHI,
S. TANAHASHI, Y. TANIGUCHI, T. TSUZUKI,

Institute of Plasma Physics, Nagoya University, Nagoya 464-01, Japan

(Received - Apr. 8, 1989)

Further communication about this report is to be sent to the Research Information Center, Institute of Plasma Physics, Nagoya University, Nagoya 464-01, Japan

IMPROVED CONFINEMENT REGIMES IN JIPP T-IIU

T. WATARI, R. KUMAZAWA, K. TOI, Y. HAMADA, A. ANDO,
Y. OKA, O. KANEKO, K. KAWAHATA, K. ADATI, R. AKIYAMA,
R. ANDO, T. AOKI, J. FUJITA, S. HIDEKUMA, S. HIROKURA,
K. IDA, H. IKEGAMI, K. KADOTA, E. KAKO, A. KARITA, Y. KAWASUMI,
S. KITAGAWA, M. KOJIMA, T. KAWAMOTO, T. KURODA, K. MASAI,
A. MOHRI, S. MORITA, K. NARIHARA, Y. OGAWA, K. OHKUBO,
S. OKAJIMA*, T. OZAKI, A. SAGARA, M. SAKAMOTO, M. SASAO, K. SATO,
K.N. SATO, T. SATO, T. SEKI, F. SHIMBO, H. TAKAHASHI,
S. TANAHASHI, Y. TANIGUCHI, T. TSUZUKI,
Institute of Plasma Physics, Nagoya University, Nagoya 464-01, Japan

ABSTRACT

The H-mode, an improved confinement regime, has been observed recently in JIPP T-IIU high power heating experiments. It was obtained in a limiter configuration without any shaping of the plasma cross-section. This H-mode is not common because it is obtained with ICRF heating. The H-mode is also obtained in a combined heating with NBI and ICRF and it is found that the threshold power level is similar to that of averaged ICRF heating.

The power threshold of the H-mode is then studied for its dependence on various plasma parameters: It increases with plasma current, insensitive to plasma density, and optimized against toroidal field intensity. The power deposition profile of ICRF heating is analyzed using a ray-tracing code, and used to explain the observed B_T dependence. This paper also deals with a class of strange shots observed

* Department of Applied Physics, Chubu University, Kasugai 487, Japan.

in the same series of experiments. They appeared at a power level close to the H-mode threshold with a remarkable improvement of confinement. However, they are different from the H-mode in the time evolution of the profiles.

1. INTRODUCTION

In previous papers [1-5], we reported on high power ICRF heating experiments, conducted on JIPP T-IIU up to 1986. The major efforts were directed toward solving the impurity problems [1,3,4] in the world-wide attempts to establish ICRF heating as a reliable heating method. Trials have been also made to improve heating efficiency by means of tailoring $k_{\parallel}$ [5], the wave number parallel to the magnetic field. As a result, 2 MW of ICRF power was successfully injected in JIPP T-IIU plasma achieving 2 MW/m^3 [1]. A severe degradation of energy confinement was found the dominant feature of such intensely heated plasmas [2], as in NBI heated plasmas [6] (L-mode). The detailed study of confinement scaling and the related profile consistency was the major subject in 1986, and these had been worked out by 1987 [2,3].

The discovery of the H-mode reported first from ASDEX [7] was a very encouraging development because the degradation of the L-mode has been so severe that the prospect for thermo-nuclear fusion was very bleak. This success was duplicated by many other machines [8-14] and it was found, as a common feature, that the presence of a divertor plays an important role and that an elongation of the plasma will help in obtaining an H-mode. Since JIPP T-IIU is a tokamak with a circular plasma cross-section small in size, there is little chance of getting H-mode. It was also reported that keeping the recycling low in the main chamber might be another prerequisite for obtaining H-modes. From this point of view, ICRF heating is not believed to be a good method of heating for obtaining an H-mode because its strong interaction at the plasma periphery is well-known, and, there have been in fact very few cases where H-mode has been obtained with ICRF heating (JFT-2M [15] and ASDEX [16]).

In spite of all these facts, H-mode transition was observed in an

experiment in 1988 on JIPP T-IIU. In 1987, JIPP T-IIU was equipped with a neutral beam injector (NBI) and ICRF power sources were reinforced. A change was also made on the high field side limiters to increase the carbonic area. It seems that these modifications worked together to make realization of the H-mode in JIPP T-IIU possible. This paper deals with this limiter H-mode. Its quality is discussed in section II. A comparison between ICRF and NBI in their abilities to facilitate H-mode is made in section III. The parametric dependence of the threshold power is studied in section IV. Finally, an aspect of the edge localized mode is discussed in section V.

In the 1988 experiment, other regimes with improved confinement were also found. Section VI is addressed to describing the characteristics of these modes.

II. CHARACTERISTICS OF JIPP T-IIU LIMITER H-MODE

JIPP T-IIU is a small tokamak with major radius R = 0.91 m and minor radius a = 0.23 m (see Fig. 1). The maximum toroidal field is 3T at the center of the plasma. Two-ion-hybrid heating is adopted in JIPP T-IIU ICRF heating where electron Landau damping is theoretically predicted to be the wave absorption mechanism. JIPP T-IIU has now eight antennas to complete the toroidal phasing, with two newly added to those used in the 1986 experiment [5]. NBI came into full operation in 1987. It is capable of injecting about 0.75 MW of net power into the plasma at an energy of 30 keV at an angle of 80° to the magnetic field. The resultant increase in power brought the device to a condition under which an H-mode is obtained more easily.

Since the axis of the vacuum chamber located at R = 93 cm and the standard position of the axis of the plasma is R = 91 cm, the plasma

touches the limiter at the inner side of the mid plane. This is the condition reported to be favorable for obtaining H-mode. This configuration was naturally employed in JIPP T-IIU in order to satisfy another requirement: It was necessary in order to couple the ICRF power to the plasma efficiently. Two carbon tiles were added in 1987 in order to increase the carbonic area, the pumping action of which is believed to be favorable in getting H-mode.

It seems useful to elucidate the wall condition under which the H-mode is obtained. As we have reported [1], JIPP T-IIU ICRF heating was much improved by carbonization. However, on a high power injection, this enhances the recycling causing disruptions in shots due to an enormous rise in density. Therefore it was always necessary to reduce the recycling after carbonization and it was by doing so that good high power heating was achieved in past experiments. The last carbonization was applied in early July 1988 and the first H-mode shot was found in October. During these three months, deuterium ECH discharge cleaning and He pulse discharge cleaning were applied occasionally. In addition, in the week the H-mode appeared for the first time Ti-gettering was applied, which has been an efficient method of reducing recycling after carbonizations. Thus we can draw a conclusion that a low recycling wall condition was being created.

Figure 2 shows a typical H-mode shot which is obtained under the condition: $B_T \sim 2.86$ T, $I_p \sim 223$ kA, and $n_e \sim 5 \times 10^{13}$. This shot makes the transition into H-phase at t = 188 ms, manifestign itself by a sudden drop in the Hα signal (Fig.2 (f)). The reduction of the Hα signal is seen in all the lines of the sight of 10-channel Hα detector array. The working gas of the discharges in this experiment is D_2 with 10% of H_2-admixture in order to facilitate ICRF heating. The detectors

are sensitive to both Dα and Hα lines. However, the signal is simply refered to as Hα-signal for brevity throughout this paper. Figure 2(b) shows electron cyclotron emission (ECE) signals representing the electron temperatures at the center and the edge. The formation of an edge electron temperature pedestal, which is another specific feature of an H-mode, is clearly observed. The electron temperature at the plasma center seems to rise slightly, being drived by the rise in edge electron temperature. As seen from the spikes in the Hα signal, the H-mode in JIPP T-IIU sufferes from so-called edge localized mode (ELM). The edge electron temperature shows ELM-sawteeth activity in inverse correlation to that of the Hα signal. The improved particle confinement and corresponding density rise is reported to be a specific feature of an H-mode. The density rise is observed in the JIPP T-IIU H-mode as well; however, it is cramped by the ELM which follows the transition (Fig.2(a)). Therefore the stored energy gain is modest, ranging from 10 to 15 percent of the level prior to transition (Fig.2(f)). Figure 2(e) shows the total injected power, showing that the H-mode threshold power is around 2.0 MW. The reaction from the ELM is also observed.

In the previous paper, which describes the L-mode characteristics, we reported that there are two phases associated with the electorn temperature profile evolution in JIPP T-IIU L-mode shots [3]. The phase referred to as the transient phase rules right after the application of the rf pulse and allows for a peaked electron temperature profile. The other phase, referred to as the constrained phase, follows it and is subject to a broader profile determined by the surface q-value. Noteworthy is that H-mode transition always occurs after the plasma goes into the constrained phase. Remarks should be made also on the plasma density range. The plasma density under which H-mode exists

extends up to 10 x 10^{13} cm^{-3} and may be higher. H-modes in other devices have density ranges lower than this. It is likely that the density scales as $B_T/R/q$ not only in L-mode but also in H-mode. This aspect may be important in designing a high B_T machine such as CIT.

III. SUPERPOSITION OF NBI AND ICRF POWER

Because H-mode have been reported for the first time (and from many devices) in connection with the use of NBI as the means of additional heating, there is no doubt that NBI is one of the most suitable heating schemes for the purpose of getting H-mode. Since JIPP T-IIU is equipped with two additional heating methods, NBI and ICRF, it is of interest to see the differences brought about by the differences in their respective power deposition profiles. The net NBI power into the plasma is limited up to 0.75 MW which alone cannot exceed the power threshold. NBI power can be used, however, in superposition on the ICRF power and break the threshold. In the shot shown in Fig.3, H-mode cannot be attained with only ICRF, and the threshold is exceeded by applying NBI. The transition occurs at 5 ms after the application of NBI, and is followed by a remarkable increase in the stored energy.

In order to get a comparison between the cases with ICRF only and NBI plus ICRF, the plots shown in Fig.4 are made. Here, stored energy is shown versus ICRF power with open circles showing L-mode shots and filled circles showing H-mode shots. It is seen in Fig.4(a), the case with ICRF only, that the stored energy increases subject to an L-mode scaling and H-mode appears with the power larger than 2 MW. The H-mode shots enclosed by a broken line are obtained only when optimized or triggered; these we will discuss briefly in sections IV and V, respectively. The increment in the stored energy on H-mode transition though small is

clearly seen. Similarly, Fig.4(b) shows the case with NBI plus ICRF power. The stored energy of the purely NBI-heated plasma is around 11 kJ and that of the Ohmic target plasma is 4 kJ. The density of the target plasma is around 2-3 x 10^{13} cm^{-3} initially, and NBI brings it up to 6 x 10^{13} cm^{-3}. By the use of Alcator scaling with this enhanced $\bar{n}_e$, the stored energy of the target plasma is estimated to be about 8 kJ. There was worry that because the NBI is injected perpendicularly, it might not have good heating quality. However, the reasonable increment in the stored energy ($\sim$ 3 kJ) shows that the NBI had enough quality. The H-mode appears in this combined heating with and ICRF power larger than 1.3 MW. All the shots are put together in Fig.5 with total power (NBI + ICRF) on the abscissa, where we assume that P_{NBI} = 0.75 MW which is the prediction of NFREYA code. We observe here that data points are on a line showing that the perpendicularly injected NBI heating is as efficient as ICRF heating. The H-mode data points become mixed at a power level higher than 2 MW, showing that there is no major difference between these two heating methods in facilitating H-mode.

IV. THRESHOLD POWER

The investigation of the dependence of the threshold power on various plasma parameters has been one of the most important areas in H-mode study. Not only it is important as a data base for new projections, but it may also provide a key for the clarification of the physics of the H-mode. This area has been worked on by many researchers and information is available from ASDEX, JFT-2M, D-IIID, PBX and JET. However, due to the variety of the parameters involved, such as the mean of plasma heating, the presence or absence of an divertor, the size of the tokamak, the intensity of the magnetic field, etc., a consistent picture has not yet

been established. The JIPP T-IIU H-mode experiment may supplement these foregoing efforts by making a specific aspect of limiter H-mode with ICRF heating.

Figure 6(a) shows the dependence of the H-mode threshold on I_p where data are taken from the parameter range satisfying 2.8 T < B_T < 2.85 T. Open circles designate L-modes and filled ones H-modes. The threshold power is obtained from the line separating them and is found to be an increasing function of I_p. This contrast with the result presented from JFT 2M [10] where it is inversely proportional to I_p.

Figure 6(b) shows the dependence of the threshold power on $\bar{n}_e$ where data are taken from the parameter ranges 2.80 T < B_T < 2.85 T and 225 kA < I_p < 234 kA. The threshold power does not depend much on $\bar{n}_e$ in the range from 4 x 10^{13} cm^{-3} to 9 x 10^{13} cm^{-3}. This is defferent from the result in D-IIID [13] where the threshold power is dependent linearly on $\bar{n}_e$. The absence of the data points with $\bar{n}_e$ below 4 x 10^{13} cm^{-3} does not always indicate the presence of so-called low density limit. This is because, the density rise occurs whenever high power is injected making it difficult to obtain the plasma at low $\bar{n}_e$.

Figure 6(c) shows how the threshold power is dependent on the plasma position, where the data are taken from the parameter ranges 2.80 T < B_T < 2.85 and 225 kA < I_p < 235 kA. From the neoclassical point of view of H-mode it has been argued that reducing the recycling in the main chamber is a necessary condition for obtaining H-mode. Indeed the importance of the clearance between the outermost flux surface and the limiter has been confirmed in every H-mode experiment. The JIPP T-IIU plasma is limited by bore limiters with radius 24 cm and top and bottom rail limiters with separation of 48 cm. The data in Fig.6(c) show that threshold power does not change when the plasma position is shifted

from R = 90 cm to 92 cm. The clearance between the plasma boundary and the limiter at the outer midplane, δ, takes a minimum value, 2.5 cm, when R = 92 cm. The requirement on δ for H-mode to be obtained is, therefore understood to be 2.5 cm. This value is similar to or a little smaller than those shown on other devices.

Figure 7 shows the dependence of the threshold power on B_T as it is changed from 2.6 to 3.0 T, where data are taken form the parameter range 225 kA < I_p < 235 kA. It is noticed that the threshold power takes on a minimum value at around B_T = 2.8 T. The B_T dependence of the threshold power has been studied in JFT-2M [10] and it was concluded that a linear dependence held. The result obtained here is very different from this. We should, however, remember that the variation of B_T is more deeply related to the variation of the power deposition profile than to the changes in the confinement system that sustain the H-mode; in this point ICRF heated plasma is very different from ones heated with NBI.

The power deposition profile has been theoretically studied for relevant plasma parameters by the use of a ray tracing code [17]. The JIPP T-IIU plasmas marginally satisfy the condition under which WKB approximation is valid. Therefore the discussion in the following is only qualitative and this is the best we can do to get the power deposition profiles. The resultant power deposion profile is shown in Fig.8 with traces of rays shown in Fig.9. We notice that by lowering the B_T from 3 T the center of the power deposition is shifted toward the larger minor radius. Thus the B_T dependence obtained in Fig.7 possibly indicates that edge plasma heating helps plasmas go into H-mode. The large threshold value for B_T < 2.75 T may be due to the enhanced impurity influx caused by the heating of the extreme edge of the plasma. To study how H-mode characteristics change according to the variation of the power deposition

profile is informative, and there are two experiments performed from this point of view: JFT2M [18] and D-IIID [19]. Both used ECH as the means of changing the profile and reached different conclusions: The threshold power is reduced by heating the edge of the plasma in JFT-2M while it is reduced by heating the core of the plasma in D-IIID. The JIPP T-IIU result is in accord with the JFT-2M result and clearer in the experimental setup in the sense that assistance of NBI is no longer necessary. However, the disadvantage of using ICRF heating for such a purpose may lie in the deleterious (impurity) effect caused by heating the very edge of the plasma.

The threshold power was examined also in the phasing of the antennas, an aspect of H-mode study specific to ICRF heating. The JIPP T-IIU vacuum vessel consists of 20 sections, one for each toroidal coils, and eight antennas are distributed as shown in Fig.1. Here we are particularly interested in the phasing where the relative phase angle of the rf current in the adjacent section $\Delta\phi$ is 0 or π. Some of the theories predict less edge interaction with $\Delta\phi = \pi$ which is one of the key requirements for an H-mode. In Fig.10 the threshold power is compared between the two cases $\Delta\phi = 0$ and $\Delta\phi = \pi$. The threshold power is slightly lower with $\Delta\phi = \pi$ than $\Delta\phi = 0$ in accord with those theoretical expectations. Our previous experimental work reports two points on the effect of antenna phasing: A little broader power deposition profile with $\Delta\phi = 0$ and a better power accountability with $\Delta\phi = \pi$. The former suggests an advantage in obtaining H-mode for $\Delta\phi = 0$ and the latter for $\Delta\phi = \pi$. These effects may be partly offsetting each other making the net effect small. The experimental result suggests that the latter aspect of the antenna phasing makes more contribution than the former in JIPP T-IIU and causes the reduction of the threshold power.

V. EDGE LOCALIZED MODE

The degree of improvement of τ_E, the figure of merit of an H-mode, is small in JIPP T-IIU. This is due to the ELM activities, which we have not succeeded in suppressing. This section will be devoted to characterizing the role of ELM in JIPP T-IIU.

It is a general feature of JIPP T-IIU experiment that the period of the ELM becomes longer if the ICRF power is reduced to a level less than the H-mode threshold after the shot goes into the H-mode. The two typical cases are shown in Fig.11. In the low I_p case shown in Fig.11(a), 1.8 MW of ICRF power is enough to exceed the H-mode threshold. The rf power is ramped down from t = 216 ms and settles to 1.0 MW at t = 224 ms. The L-mode transition occurs at t = 222 ms when ICRF power is reduced to about 1.1 MW. This means that the power needed to sustain the H-mode is much lower than that necessary to initiate the H-mode. The presence of such triggered H-mode or hysteresis is known to be common to all phase transition phenomena. It is interesting to point out that the stored energy keeps the same value while the rf power is being ramped down from 1.8 MW to 1.1 MW. This suggests that the comfinement has been improved by 1.7 times. The improvement of the confinement is in a good correlation to the reduced frequency of the ELM: For the time span from t = 205 ms to 216 ms where full power (1.8 MW) is injected, the ELM occured with a period fo 1.37 ms. Presumably, about 2.3 kJ of the plasma stored energy is carried away by each occurence of ELM. While the power is being ramped down the ELM-period is about 2 ms. Assuming that the same amount of the energy is lost for each ELM, 1.1 MW of the power is calculated to be dissipated in ELM. This almost accounts for the applied ICRF power. Similarly in the high I_p case shown in Fig.11(b), the H-mode is attained at a higher power level of 2.3 MW. The rf power

is then turned down to 1.7 MW at t = 285 msec. The stored energy keeps a constant value indicating a confinement improved 1.35 times. Each ELM is presumed to dissipate 2.3 kJ with a period of 1.0 ms at the high power level. With the longer period of 1.6 ms at the lower power level, the energy loss due to ELM is estimated to be 1.4 MW by similar arithmetics. This accounts well for the most of the injected energy.

Such an observation leads us to an understanding of the situation, where JIPP T-IIU H-mode is influenced by ELM activities. In Fig.12, τ_E is shown schematically as dependent on the injection power where τ_E^L is a L-mode τ_E like that given by Kaye-Goldston scaling and τ_E^H is the H-mode τ_E which is usually taken to be three times larger than that of L-mode. If the H-L transition belongs to the family of general phase transition phenomena, these different τ_E should be bridged by a hysteresis curve. On the other hand ELM seems to occur so as to softly limit the plasma stored energy. This imposes an interrelation $\tau_E^* P = W_p^{max}$ between τ_E^*, the practical τ_E, and P, the injected power, with W_p^{max}, the maximum stored energy. These two curves are inferred to cross each other for the JIPP T-IIU case in a way as shown in Fig.12. Since $\tau_E^H > \tau_E^*$ in any range of P, there is no chance of obtaining an ELM-less H-mode and τ_E^* is actually realized. The ELM also seems to occur in order to trim the edge electron temperature, a measure of ∇T_e at the plasma edge (see Fig.2(b)). With profile consistency [20] assumed, the cramped stored energy is more adequately interpreted as a consequence of the cramped edge pressured gradient, ∇P. Thus on the basis of the Wesson-Sykes local expression [21],

$$W_p^{max} \propto \nabla P|_{edge}^{max} = \frac{1}{1.67} \frac{B_T^2}{2\mu_0} \frac{1}{q^2} \frac{1}{R} S|_{edge} \qquad (1)$$

with

$$S = \frac{r}{q} \frac{dq}{dr}$$

With the high shear at the edge of the plasma, which would be obtained with a divertor or an elongation of the plasma cross-section, W_p^{max} could be larger so that $\tau_E^H < \tau_E^*$. This may be the reason why ELM-less H-mode is obtained with those configurations. Here in JIPP T-IIU, τ_E^* and S are more subject to self-organization and the integrated form

$$W_p^{max} = C \frac{B_T^2}{2\mu_0} \frac{3}{2} V_p \frac{I_p}{aB_T} \qquad (2)$$

would better fit the data. In an experiment where I_p is varied the independency of C on I_p has been confirmed. This indirectly supports the model of ELM based on the first ballooning mode stability limit. The constant C is determined to be 1.3, which is one half of the theoretical value [21]. Note should be made however that current-driven instability is not eliminated as a possible cause of ELM, because the process of self-organization imposes a constraint in turn on the current profile.

Such a phenomenological model of the ELM predicts for JIPP T-IIU that data points will be found in the shaded region in Fig.12. The projection of this area on the W_p-P plane will obviously explain the way H-and-L mode data points are distributed in Fig.5. Now that H-mode is obtained even in a plasma with a circular plasma cross section, the role of the magnetic shear should be considered with more emphasis on its role in sustaining H-mode rather than in reaching it.

VI. STRANGE SHOTS

Nuclear fusion research was encouraged by the discovery of the H-mode because the dreadful degradation of energy confinement had been frustrating the researchers. H-mode was confirmed in various machines

and investigations are going on to clarify the mechanism. Since then, a series of modes with improved confinement has been reported to exist. They are classified in a different category from H-mode and include super-shot in TFTR [22], improved Divertor Confinement in JT-60 [14], improved L-mode in JFT-2M [23], and counter-injection in ASDEX [24].

Improved energy confinement regimes which seem to belong to this family were also found in the JIPP T-IIU experiment in late 1988 and they were named strange shots. There are two types of strange shot: type-A and type-B. A representative shot is chosen from each type and displayed in Fig.13 in a way which shows their potential usefullness. In the shot shown in Fig.13(b), both NBI and ICRF are applied. When they overlap, the total power amounts to 2.75 MW, raising the stored energy to 21 kJ. The S-mode transition occurs after NBI is turned off, and the stored energy recovers to its previous level. The two types of the strange shot seems similar to each other in their remarkable increment in the stored energy and the neutron yield. However, they are different in the details of the time evolution of other plasma parameters.

Figure 14 shows the time evolution of the Type-A strange shots which are labeled by [illegible] shown in Fig.5. They appear at a power level comparable to the H-mode threshold. The outstanding feature of these shots is in the sudden improvement of the energy confinement time as observed in the enhanced stored enregy (Fig.14(f)). In this shot, the applied rf power is around 2.3 MW (Fig.13(e)) exceeding the H-mode threshold power. The improvement of τ_E is correlated with an improvement in particle confinement; as shown in Fig.14(a) the plasma density starts to rise at t = 230 ms though gas is puffed at a constant rate until t = 270 ms. For this type of strange shot, there are some signs of the presence of the triggering mechanism. We find a hump in the H_α signal

(Fig.14(f))', oneturn voltage (Fig.14(c)) and a sudden reduction of the edge magnetic fluctuation (Fig.14(e)) at t = 230 ms. The edge electron temperature drops coincident to this keeping the central electron temperature unchanged (Fig.14(b)). There must have been some event like the fall of a small carbon fragment. However, at the later stage of the RF pulse, these events are over and only the peaked electron temperature profile and the improved energy confinement persist.

Type-B of the strange shot was obtained with I_p around 260 kA. As shown in Fig.15, this mode is attained with ICRF power just below the H-mode threshold. The time evolution of one of these shots is shown in Fig.16. The gradual transition to an improved confinement as observed in Fig.16(f) is the characteristic feature of this type of strange shot. This is correlated to an improvement in particle confinement as observed in Fig.16(a). The plasma density begins to increase at the same time in spite of the fact that the gas-puffing rate is kept constant, and there is no change in the Hα signals. The electron temperature profile stays similar to that of L-mode and there are no signs of change in other signals corresponding to the transition. The improvement in the particle confinement is solely related to the improved energy confinement in this type of strange shot. The time scale of this transition is so long that we miss the steady state even with the 100 msec of the RF pulse. With a longer pulse more improvement of the confinement would be recorded. It has been reported in a wide range of takamak experiments that an improvement in particle confinement is often accompanied by an impurity accumulation. Of interest is that the same thing occurs in the strange shots as shown in the bolometer signal in Fig.16(b).

CONCLUSIONS

H-mode transition was observed in the JIPP T-IIU high power heating experiment. This H-mode is similar to and distinguished from those in other devices in the following ways: It was obtained with a limiter configuration without any shaping of the plasma cross section. It was obtained with ICRF heating only which has not been sufficiently demonstrated to be compatible with H-mode. Another feature of the JIPP T-IIU H-mode is that it is obtained at relatively high B_T despite the minimum size of the tokamak. Therefore the H-mode was attained with high density exceeding 10^{14} cm^{-3}. This H-mode is accompanied, however, by ELM activities and the energy gain was only about 10 to 15 percent. The power threshold was studied and found to be an increasing function of I_p, independent of $\bar{n}_e$, and optimized against B_T. Some of these results are in contradiction to those reported in other papers. The B_T dependence can be explained in terms of the power deposition profile change. The H-mode was also obtained with NBI superposed and a similar value of the threshold power was obtained. However, in a very optimized condition, the H-mode threshold of ICRF heated plasma is lower than that of NBI heated plasma. In an attempt to improve the H-mode characteristics by optimizing the antenna phasing, it was found that the threshold power is lower with $\Delta\phi = \pi$ than wiht $\Delta\phi = 0$.

It was found that the power necessary to sustain an H-phase is lower than that needed to reach it. By the presence of this hysterysis, H-L transition manifests itself to be one of general phase transition phenomena. Another observation of interest is the reduction of the frequency of the ELM as the power is reduced. The ELM seems to occur in order to softly limit the stored energy. Thus it was possible to improve H-mode τ_E by reducing the power below the threshold after the

plasma goes into H-phase. ELM is observed to occur as well so as to limit the edge electron temperature gradient. This interpretation should be more to the point and suggests an importance of the magnetic shear at the edge of the plasma, with which strength of the magnetic structure against MHD stability is ensured.

Different types of confinement improvement, strange shots, were observed in the JIPP T-IIU experiment. They appear at a power level close to the H-mode threshold, accompanied by an improvement in particle confinement. They are distinguished from H-modes because they have peaked electron temperature profiles contrasting to those of H-mode.

REFERENCES

[1] WATARI, T., OHKUBO, K., AKIYAMA, R., et al., in plasma physics and Controlled Nuclear Fusion research (Proc. 11th Int. Conf. Kyoto, 1986) Vol 1, IAEA Vienna (1987) 495.

[2] IDA, K., OGAWA, Y., TOI, K., et al., IPPJ-886 (1988).

[3] OGAWA, Y., MASAI, K., WATARI, T., et al., IPPJ-903 (1989).

[4] NODA, N., OGAWA, Y., MASAI, K., et al., Japanese Journal of Applied Physics, 25 (1986) 379 .

[5] ANDO, R., KAKO, E., OGAWA, Y., et al., Nucl. Fusion 28 (1988) 577 .

[6] KAYE, S.M., and GOLDSTON, R.J., Nucl. Fusion 25 (1985) 65.

[7] WAGNER, F.W., BECKER, G., BEHRINGER, K., et al., Phys. Rev. Lett., 49 (1982) 1408.

[8] KAYE, S.M., BELL, M.G., BOL, K., et al., Phys. Rev. Lett., 49 (1982)115 .

[9] OHYABU, N., BURREL, K.H., DeBOO, J., et al., Nucle. Fusion, 25(1985)49 .

[10] ODAJIMA, K., FUNAHASHI, A., HOSHINO, K., et al., in Plasma Physics and Controlled Nuclear Fusion Research (Proc. 11th Int. Conf. Kyoto, 1986) Vol 1, IAEA Vienna (1987) 151.

[11] TANGA, A., BARTLETT, D.V., BEHRINGER, K., et al., in Plasma Physics and Controlled Nuclear Fusion Research (Proc. 11th Int. Conf. Kyoto, 1986) Vol 1, IAEA Vienna (1987) 65.

[12] OKABAYASHI, M., BOL, K., CHANCE, M., et al., in Plasma Physics and Controlled Nuclear Fusion Research (Proc. 11th Int. Conf. Kyoto, 1986) Vol 1, IAEA Vienna (1987) 275.

[13] BURRELL, K. H., ALLEN, S.L., BRAMSON, G., et al., in Proc. of 12th International Conf. on Plasma Physics and Controlled Nuclear Fusion Research, Nice, 1988 CN-50/A-3-4.

[14] AIKAWA, H., AKAOKA, N., AKASAKA, H., et al., in Proc. of 12th International Conf. on Plasma Physics and Controlled Nuclear Fusion Research, Nice, 1988, CN-50/A-1-4

[15] MATSUMOTO, H., OGAWA, T., TAMAI, H., et al., Nucl. Fusion 27 (1987) 1181.

[16] STEINMETZ, K., NOTERDAME, J.M., WAGNER, F., et al., Phys. Rev. Lett. 58 (1987) 124.

[17] MCVEY, B.D., Nucl. Fusion 19 (1979) 461.

[18] HOSHINO, K., YAMAMOTO, T., SUZUKI, N., et al., Nucl. Fusion Lett. 28 (1988) 301.

[19] HARVEY, R.W., in presentation at IAEA Technical Committee Meeting, 1987, Moscow.

[20] COPPI, B., Comments Plasma Phys. Cont. Fusion 5 (1980) 261.

[21] WESSON, J.A., SYKES, A., Nucl. Fusion 25 (1985) 85.

[22] HAWRYLUK, R.J., ARUNASALAM, V., BELL, M.G., et al., in Plasma Physics and Controlled Nuclear Fusion Research (Proc. 11th Int. Conf. Kyoto, 1986) Vol.1, IAEA, Vienna (1987) 51.

[23] MORI, M., SUZUKI, N., UESUGI, T., et al., Nucl. Fusion Lett. 28 (1988) 1892.

[24] GEHRE, O., GRUBER, O., MURMANN, H.D., et al., Phys. Rev. Lett., 60 (1988) 1502.

FIGURE CAPTIONS

Fig. 1. The JIPP T-IIU machine: The locations of ICRF antennas, arrangement of carbon limiters, and the location of Ti-sublimators are shown. The NBI system has a nearly perpendicular injection angle. The phase difference between the adjacent antennas is usually chosen from π, 0, $\pm \pi/2$ so that the same phase angle is obtained as it turns around the torus.

Fig. 2. A typical H-mode shot obtained with ICRF heating: (a); plasma density and gas puffing rate. (b); electron temperature at the center of the plasma and at the edge. (c); plasma current and loop voltage. (d); bolometer signal. (e); ICRF power and rectified magnetic probe signal. (f); stored energy and Hα signal at the edge.

Fig. 3. The H-mode obtained with NBI superposed on ICRF heating: (a); stored energy and Hα signal at the edge of the plasma. (b); ICRF power and absorbed NBI power.

Fig. 4. Stored energy versus ICRF power for two cases: (a) ICRF only and (b) NBI + ICRF together. The stored energy of OH target plasma and NBI heated plasma is read out on the ordinate of figure (b).

Fig. 5. The stored energy versus total power, $P_{NBI} + P_{ICRF}$. $P_{NBI} = 0.75$ MW was assumed according to the NFREYA code result. The filled circles denote H-mode, open circles denote L-mode, and filled circles with mark S denote strange shots.

Fig. 6. The dependences of the threshold power on various parameters: (a); I_p dependence. (b); $\bar{n}_e$ dependence (c); The dependence on the plasma position.

Fig. 7. The dependence of the threshold power on the toroidal magnetic field. The minimum threshold power is obtained at around 2.8 T.

Fig. 8. The calculated power deposition profiles: The center of the power deposition shifts toward the large nimor radius side when B_T is reduced. solid line: absorption by electrons, dotted line: absorption by high energy component of deuterium, and chain-dotted line: absorption by hydrogen ions.

Fig. 9. The ICRF wave ray trajectories as waves are emanating from the high field side: (a); for B_T = 2.6 T and (b); B_T = 3.0 T.

Fig. 10. The comparison of the threshold power for the two specific phasings, $\Delta\phi = \pi$ and $\Delta\phi = 0$.

Fig. 11. Two typical shots which show the reduction of the frequency of the ELM when ICRF power is reduced after H-mode transition. The stored energy holds the value before the reduction in power. (a); a case with low I_p and P_{ICRF} ramped down. (b); a case with high I_p and adrupt reduction of P_{ICRF}.

Fig. 12. A drawing which shows the relation between the role of ELM and τ_E. The quality of the H-mode is determined by the interrelationship of τ_E^L (the L-mode τ_E), τ_E^H (the H-mode τ_E), and τ_E^* (the practical τ_E). The latter is postulated to be concerned with the strength of the edge structure against MHD stability. The τ_E^* may be larger with high shear of a magnetic field as shown imaginarily by the chain-dotted line.

Fig. 13. The two representative strange shots: (a); type-A strange shot. (b); type-B strange shot. Though type-B strange is chosen here from the case with NBI plus ICRF, NBI is not always necessary.

Fig. 14. The time evolution of various plasma parameters in a type-A strange shot: (a) gas puff rate and plasma density, (b) central and edge electron temperature, (c) plasma current and loop valtage, (d) line intensity of CII line and bolometer signal, (e) ICRF power and rectified magnetic probe signal, (f) stored energy and Hα signal at the plasma edge.

Fig. 15. Stored energy versus injected power for the high I_p case: It is observed that the H-mode power threshold is higher for this case and the stored energy is higher than those shown in Fig. 5. The different kind of strange shots (type-B) are mapped in this graph with mark S.

Fig. 16. The time evolution of various plasma parameters in a type-B strange shot: (a) gas puffing rate and plasma density, (b) the central and edge electron temperature, (c) plasma current and loop voltage, (d) line intensity of CII and bolometer signal, (e) ICRF power and the rectified magnetic probe signal, (f) stored energy and Hα signal at the edge.

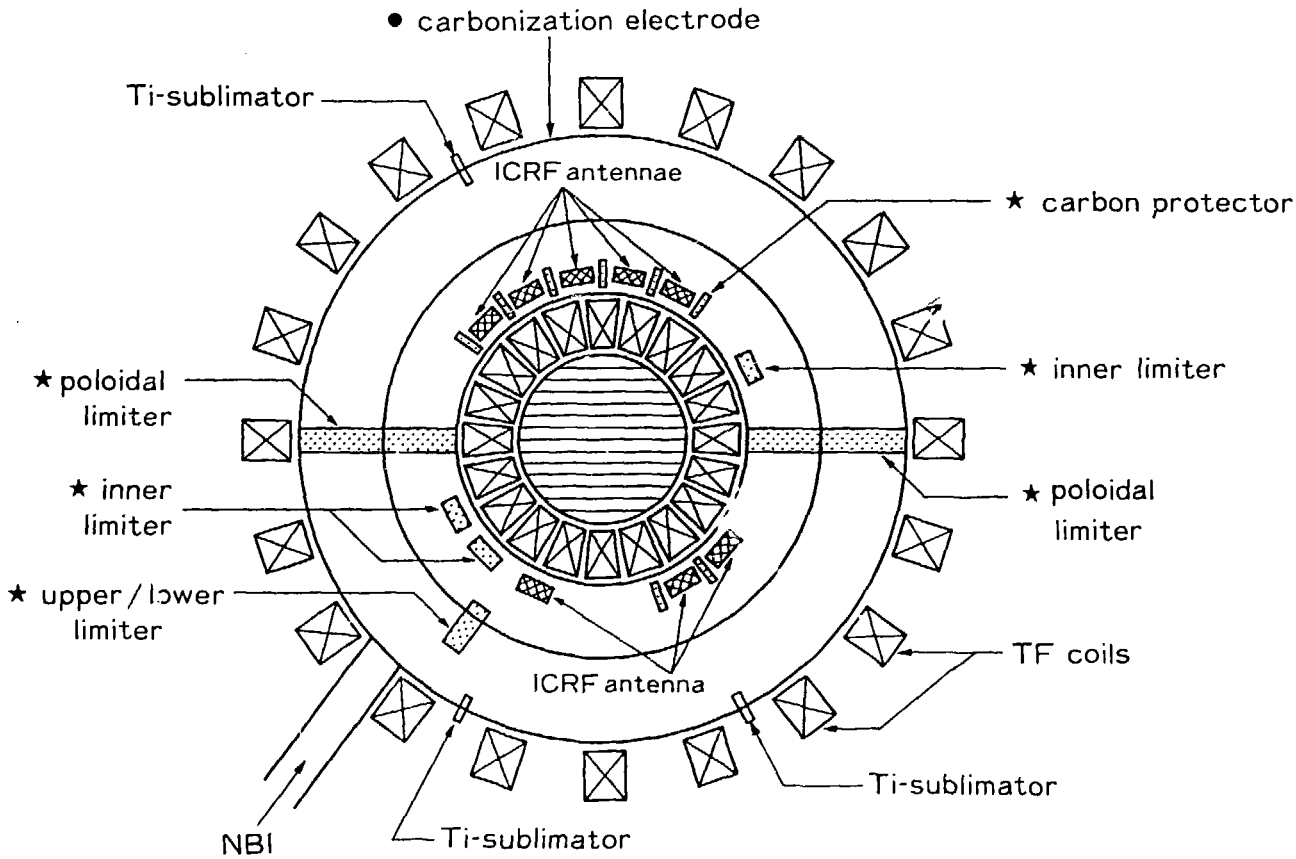
● carbonization electrode
Ti-sublimator
ICRF antennae
★ carbon protector
★ poloidal limiter
★ inner limiter
★ inner limiter
★ poloidal limiter
★ upper / lower limiter
TF coils
ICRF antenna
Ti-sublimator
NBI
Ti-sublimator

Fig.1

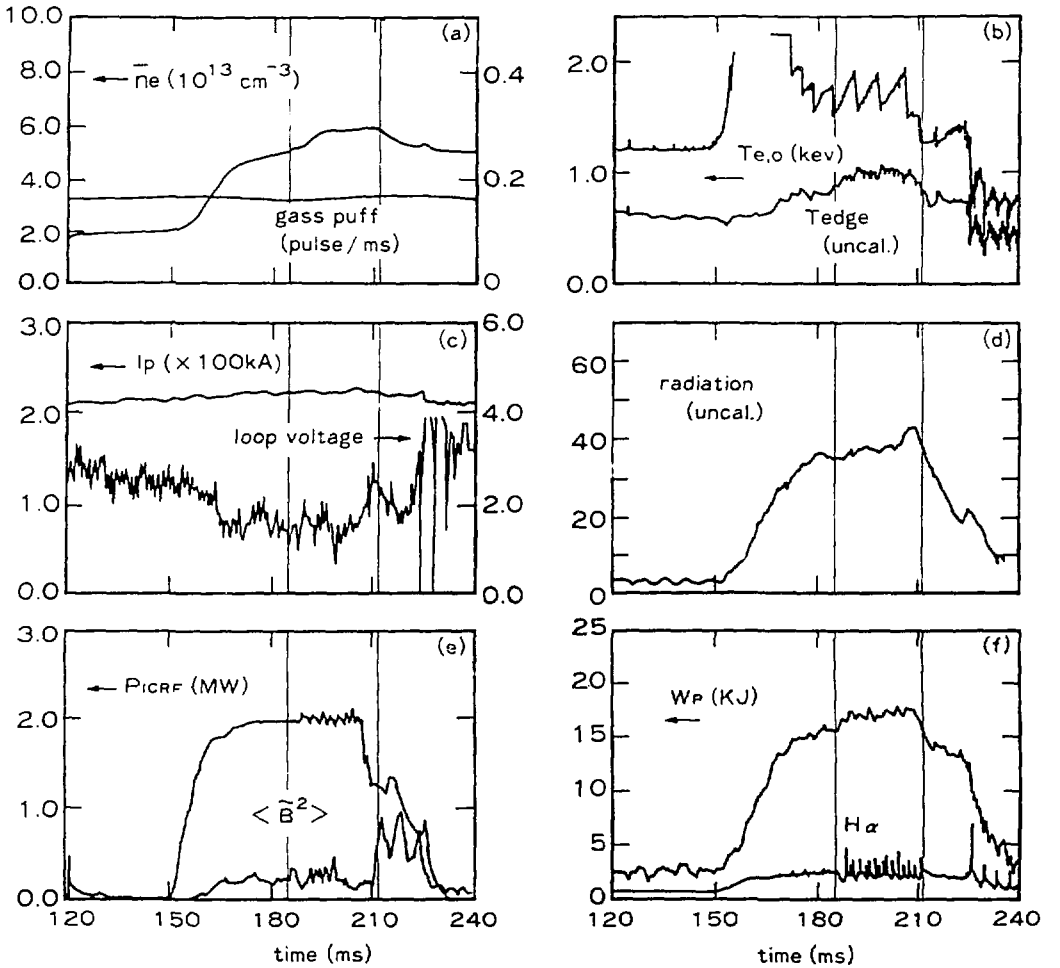
(a)
$\bar{n}e$ (10^{13} cm^{-3})
gass puff
(pulse / ms)
(b)
Te,o (kev)
Tedge
(uncal.)
(c)
Ip (×100kA)
loop voltage
(d)
radiation
(uncal.)
(e)
PICRF (MW)
$<\tilde{B}^2>$
(f)
WP (KJ)
Hα
time (ms)
time (ms)

Fig.2

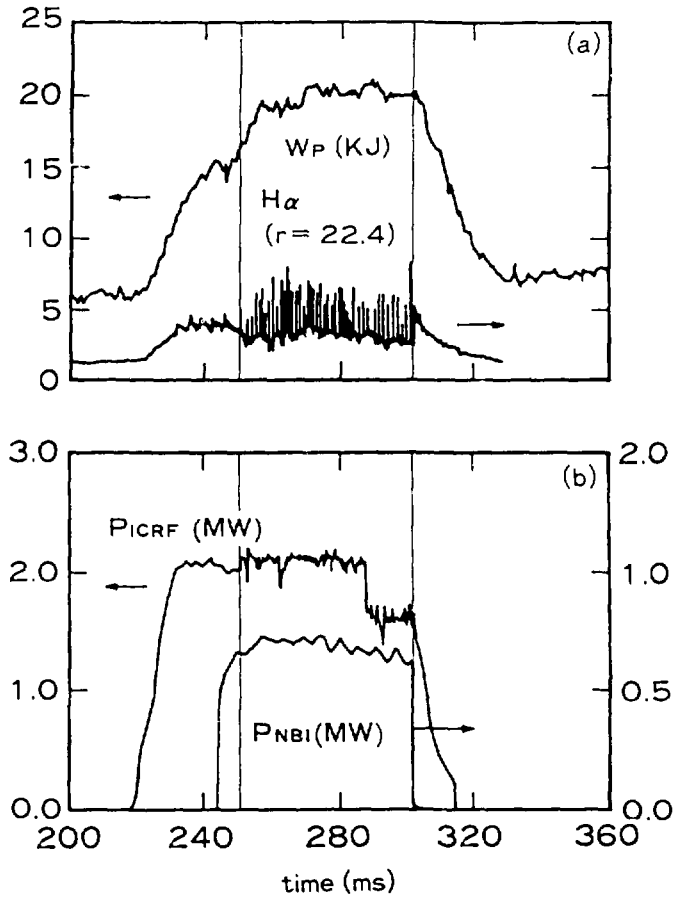
25
20
15
10
5
0
(a)
WP (KJ)
Hα
(r= 22.4)
3.0
2.0
1.0
0.0
2.0
1.0
0.5
0.0
(b)
PICRF (MW)
PNBI(MW)
200
240
280
320
360
time (ms)

Fig.3

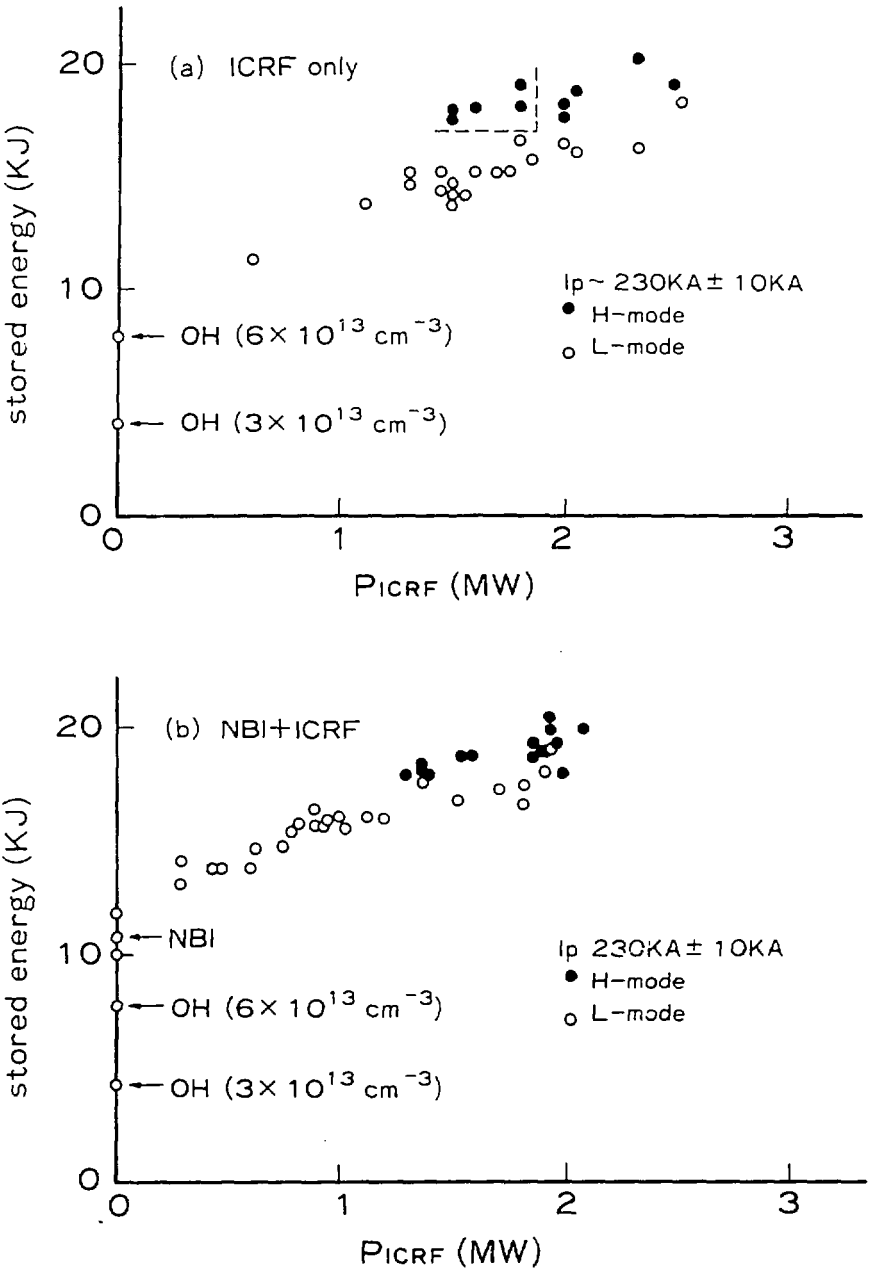
(a) ICRF only
stored energy (KJ)
20
10
0
OH (6× 10^13 cm^-3)
OH (3× 10^13 cm^-3)
Ip~ 230KA± 10KA
H-mode
L-mode
0
1
2
3
PICRF (MW)
(b) NBI+ICRF
NBI
OH (6× 10^13 cm^-3)
OH (3× 10^13 cm^-3)
Ip 230KA± 10KA
H-mode
L-mode

Fig.4

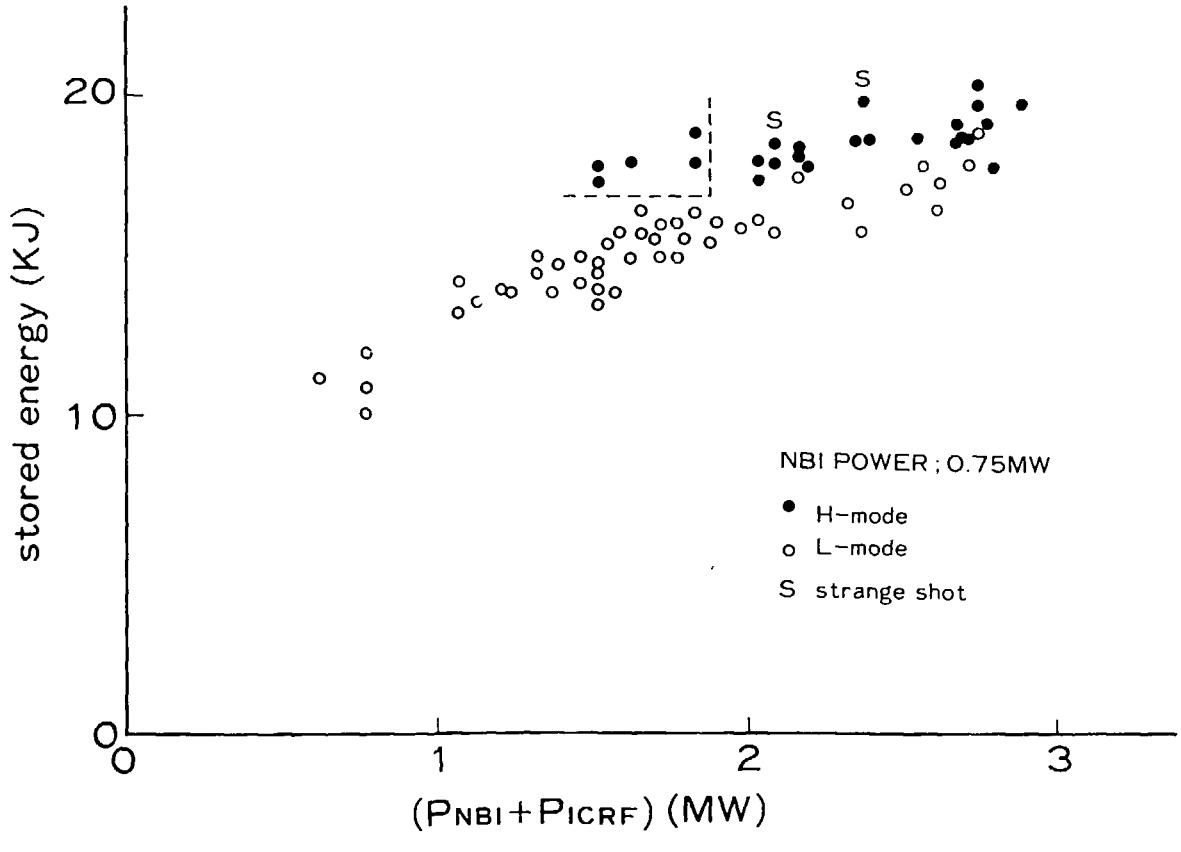
20
10
0
0
1
2
3
stored energy (KJ)
(PNBI+PICRF) (MW)
S
S
S
NBI POWER ; 0.75MW
H-mode
L-mode
S strange shot

Fig.5

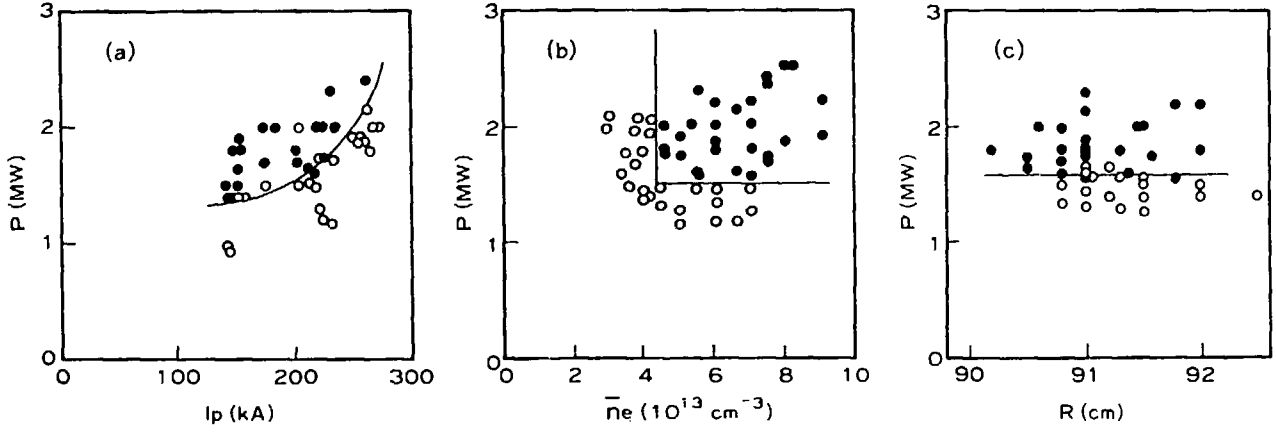
(a)
P (MW)
Ip (kA)
0
100
200
300
1
2
3
(b)
P (MW)
$\bar{n}e$ (10^{13} cm^{-3})
0
2
4
6
8
10
1
2
3
(c)
P (MW)
R (cm)
90
91
92
1
2
3

Fig.6

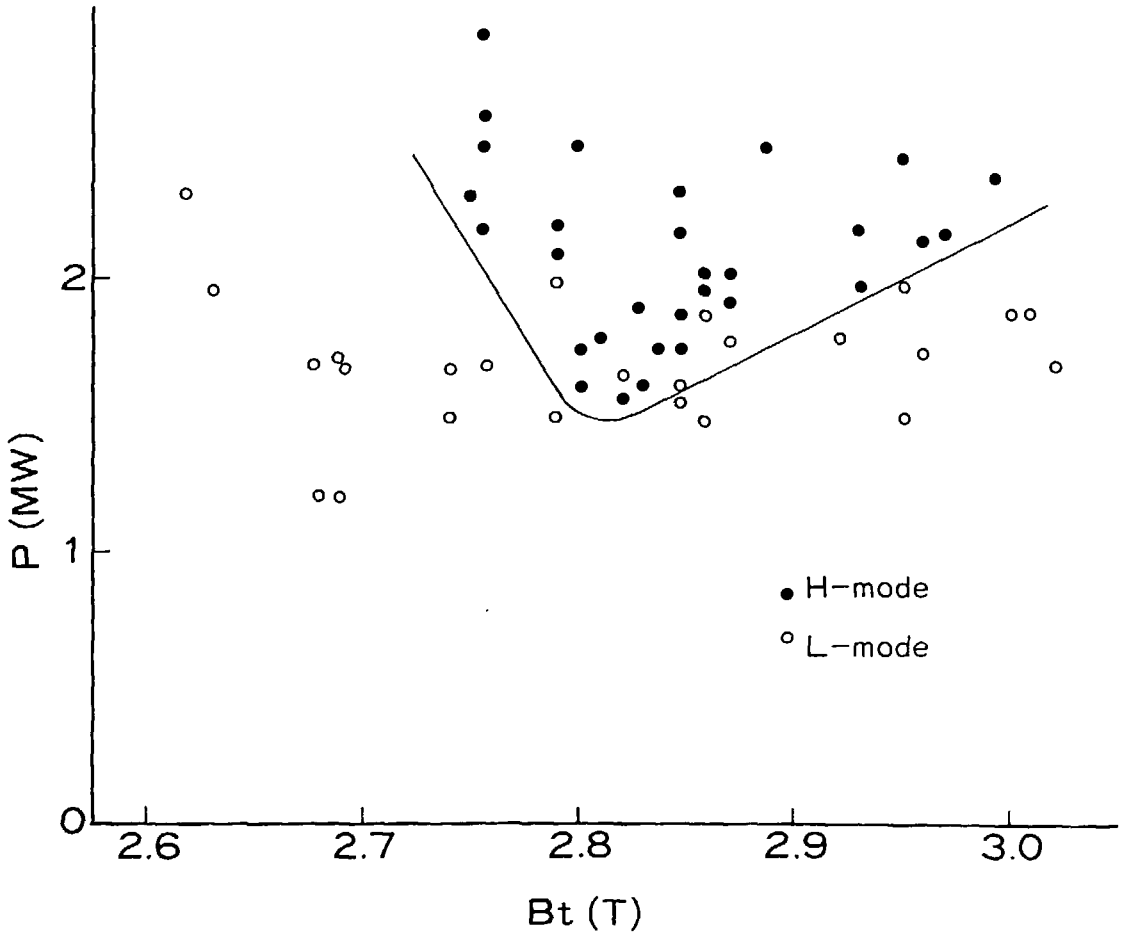

Fig.7

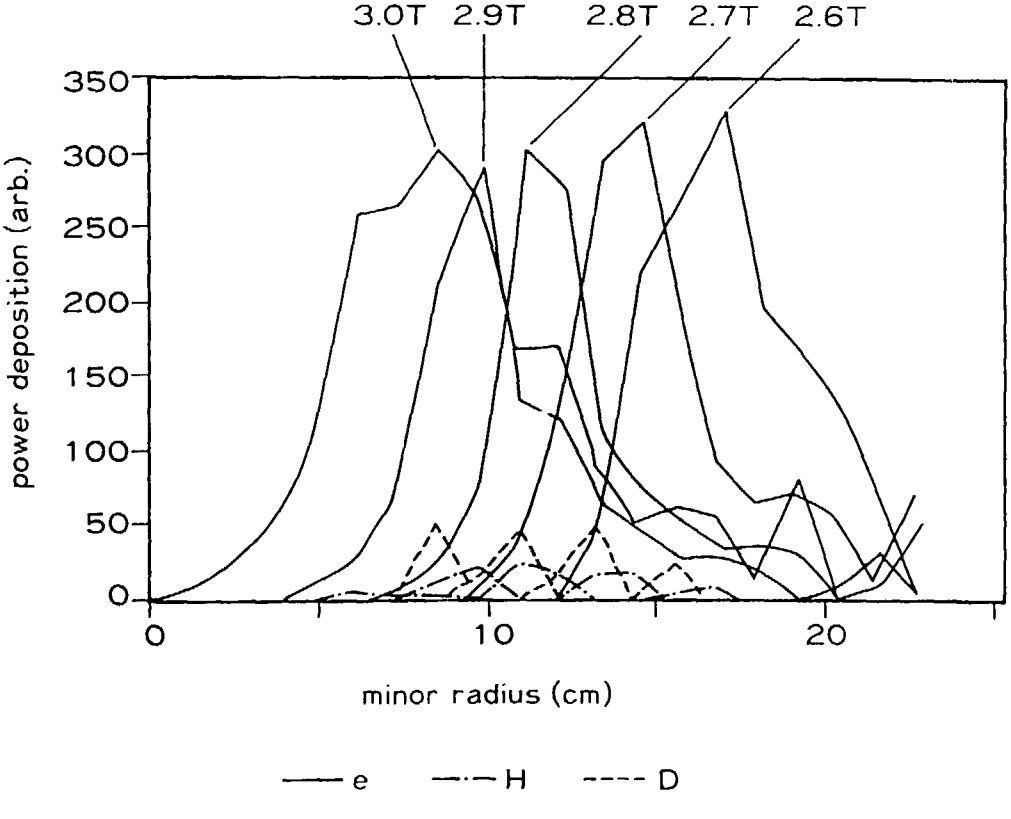
3.0T
2.9T
2.8T
2.7T
2.6T
350
300
250
200
150
100
50
0
power deposition (arb.)
0
10
20
minor radius (cm)
e
H
D

Fig.8

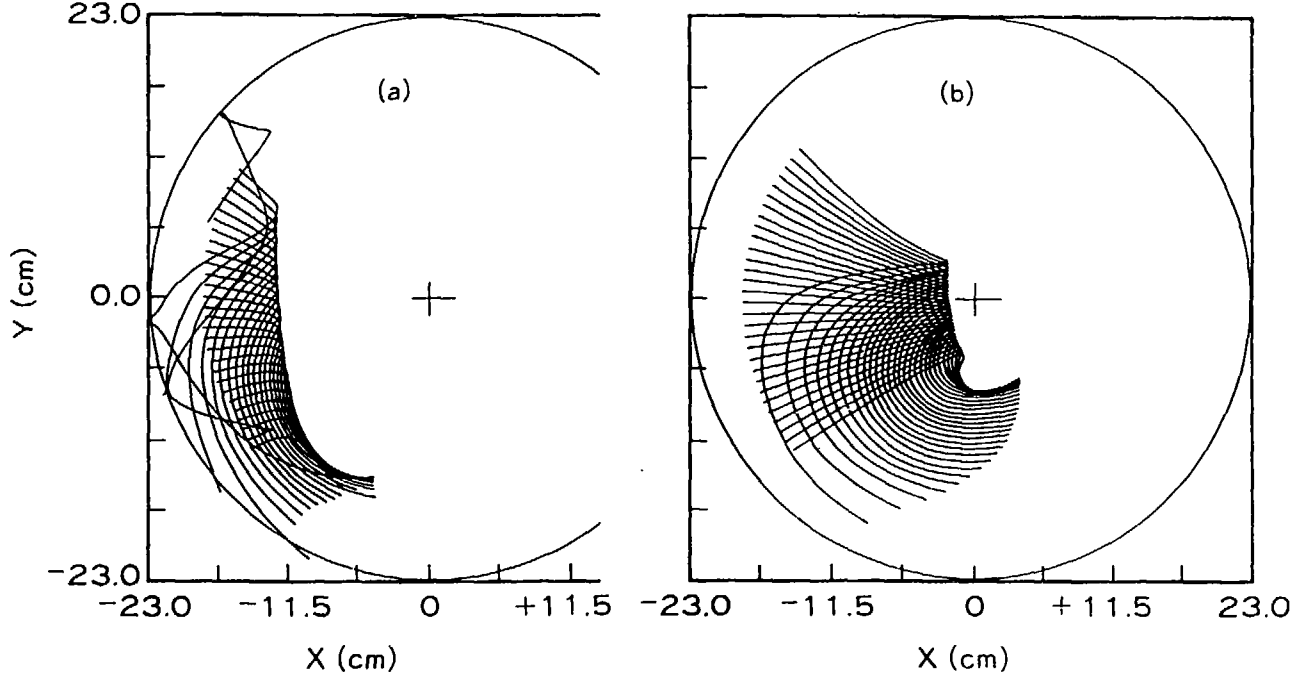

Fig.9

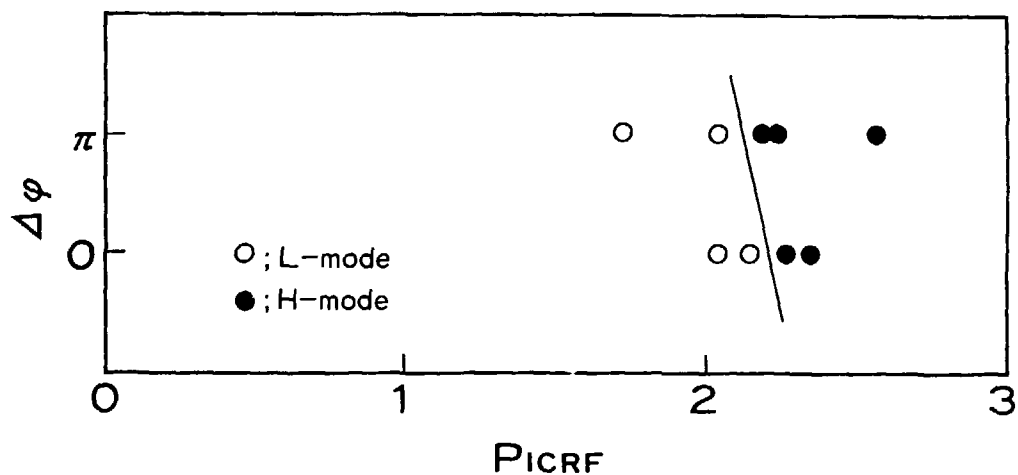

Fig.10

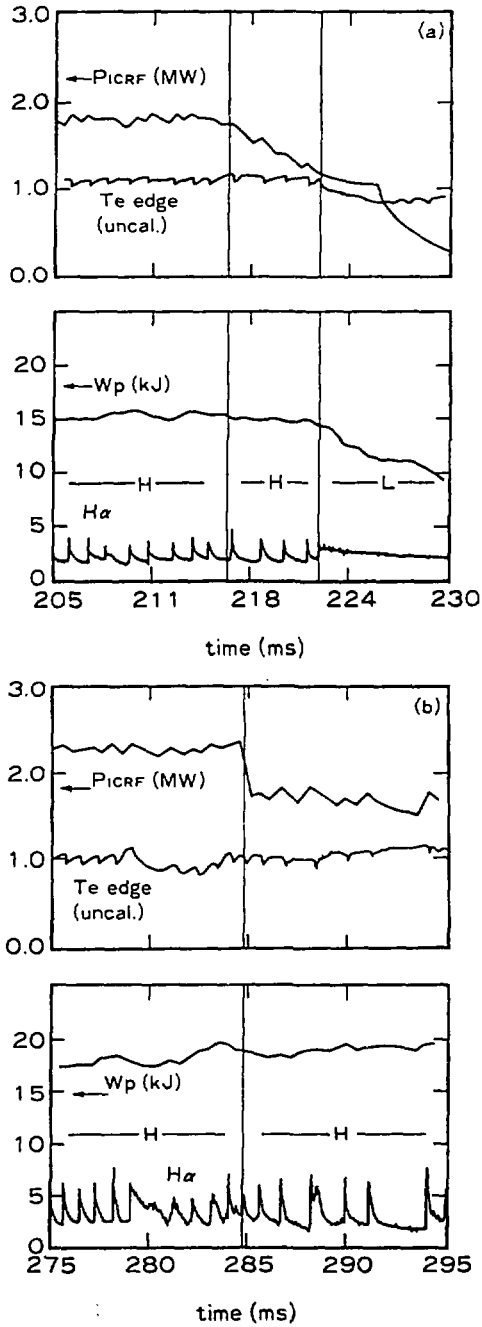
(a)
PICRF (MW)
Te edge
(uncal.)
Wp (kJ)
H
H
L
Hα
time (ms)
(b)
PICRF (MW)
Te edge
(uncal.)
Wp (kJ)
H
H
Hα
time (ms)

Fig.11

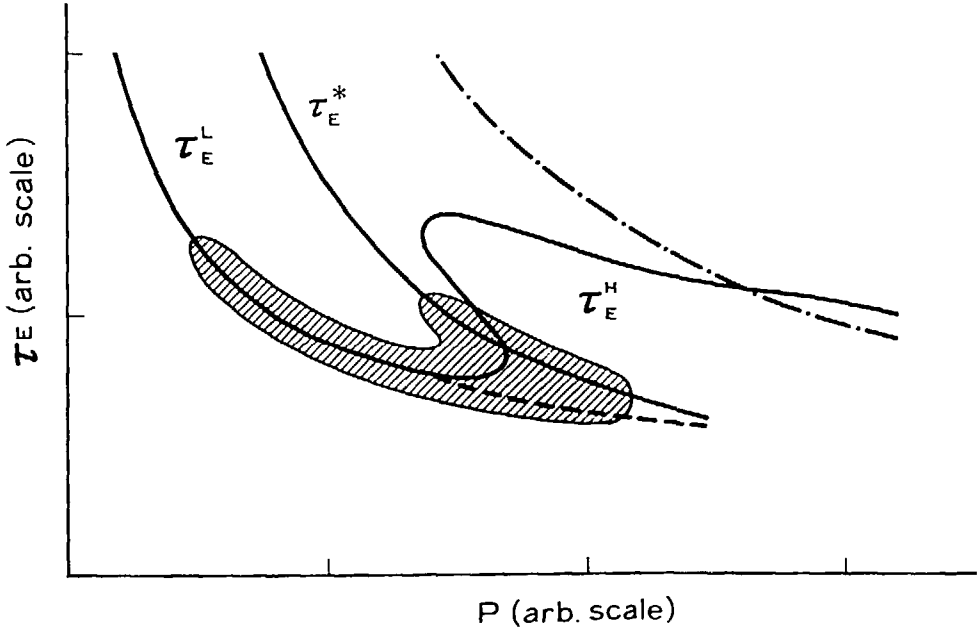

Fig.12

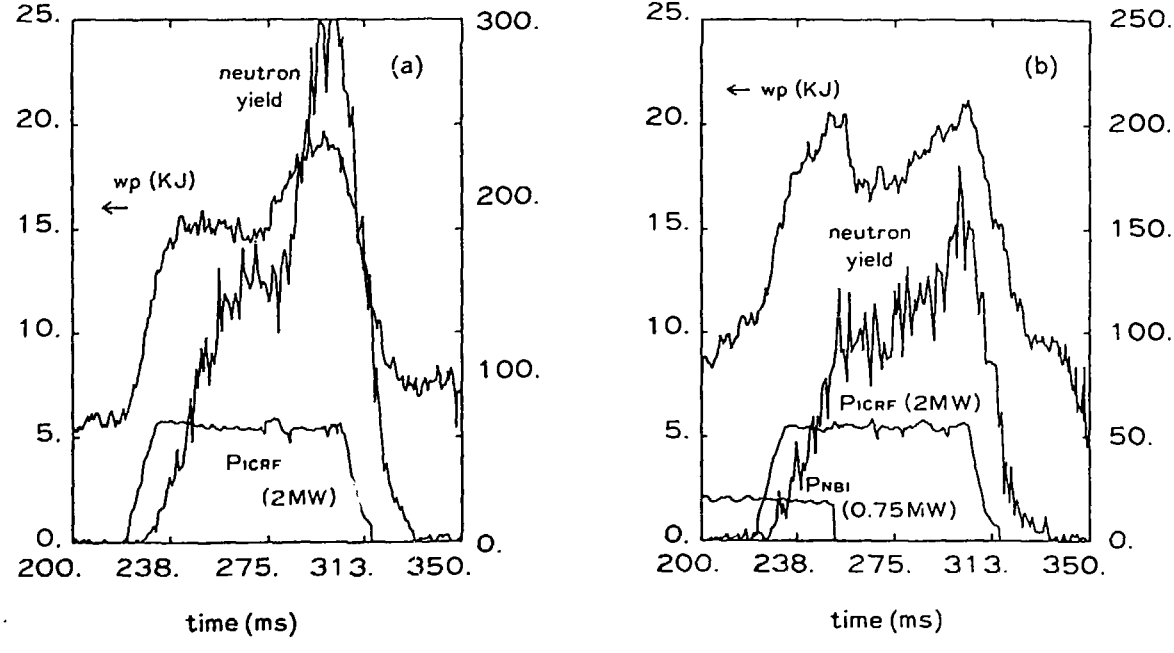
25.
20.
15.
10.
5.
0.
300.
200.
100.
0.
neutron
yield
(a)
wp (KJ)
←
PICRF
(2MW)
200.
238.
275.
313.
350.
time (ms)
250.
150.
50.
(b)
← wp (KJ)
PICRF (2MW)
PNBI
(0.75MW)

Fig.13

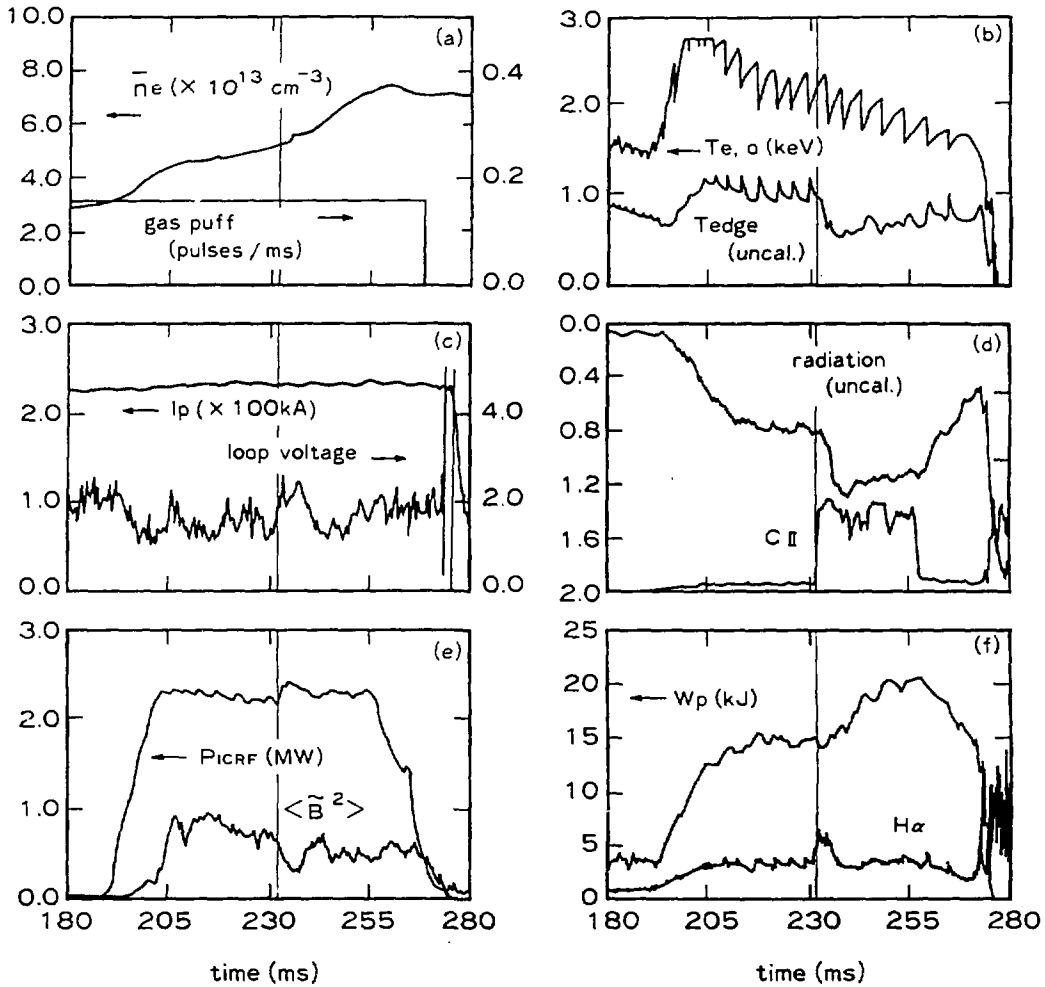
(a)
$\bar{n}e$ (× 10^{13} cm^{-3})
gas puff
(pulses / ms)
(b)
Te, o (keV)
Tedge
(uncal.)
(c)
Ip (× 100kA)
loop voltage
(d)
radiation
(uncal.)
C II
(e)
PICRF (MW)
$<\tilde{B}^2>$
(f)
Wp (kJ)
Hα
time (ms)
time (ms)

Fig.14

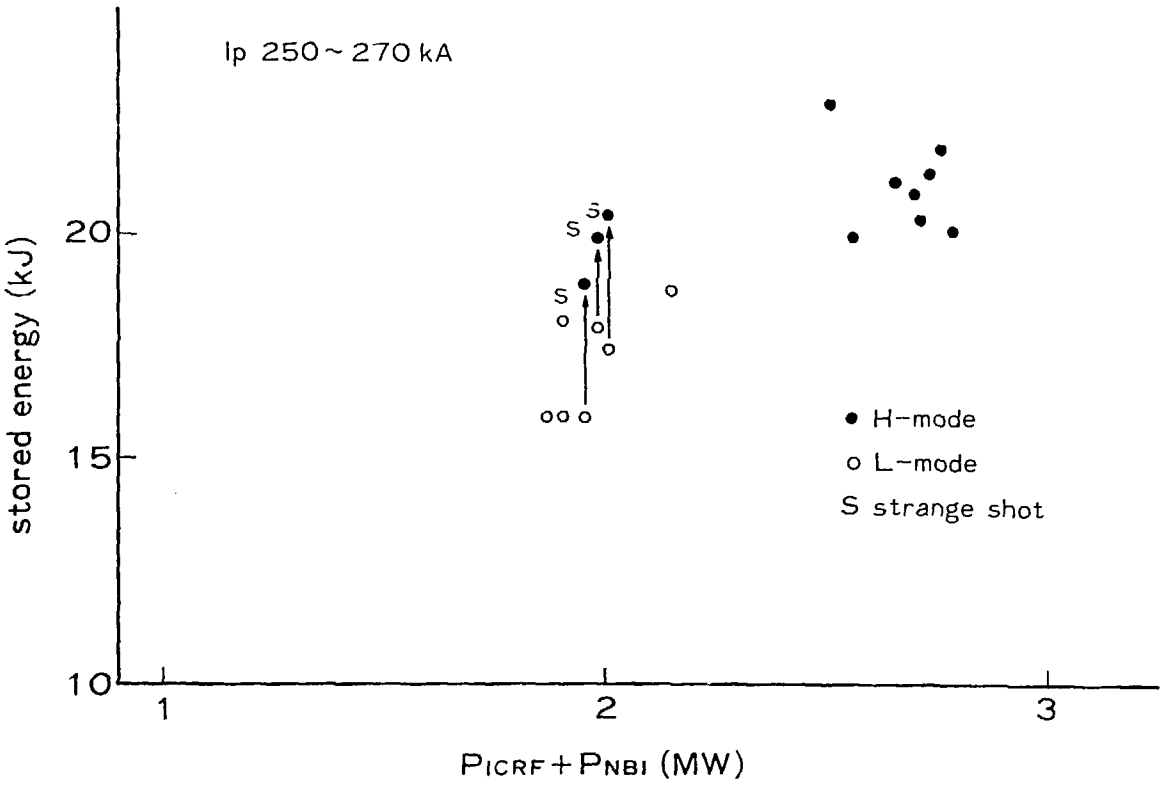
Ip 250~270 kA
stored energy (kJ)
20
15
10
1
2
3
PICRF+PNBI (MW)
S
S
S
H-mode
L-mode
S strange shot

Fig.15

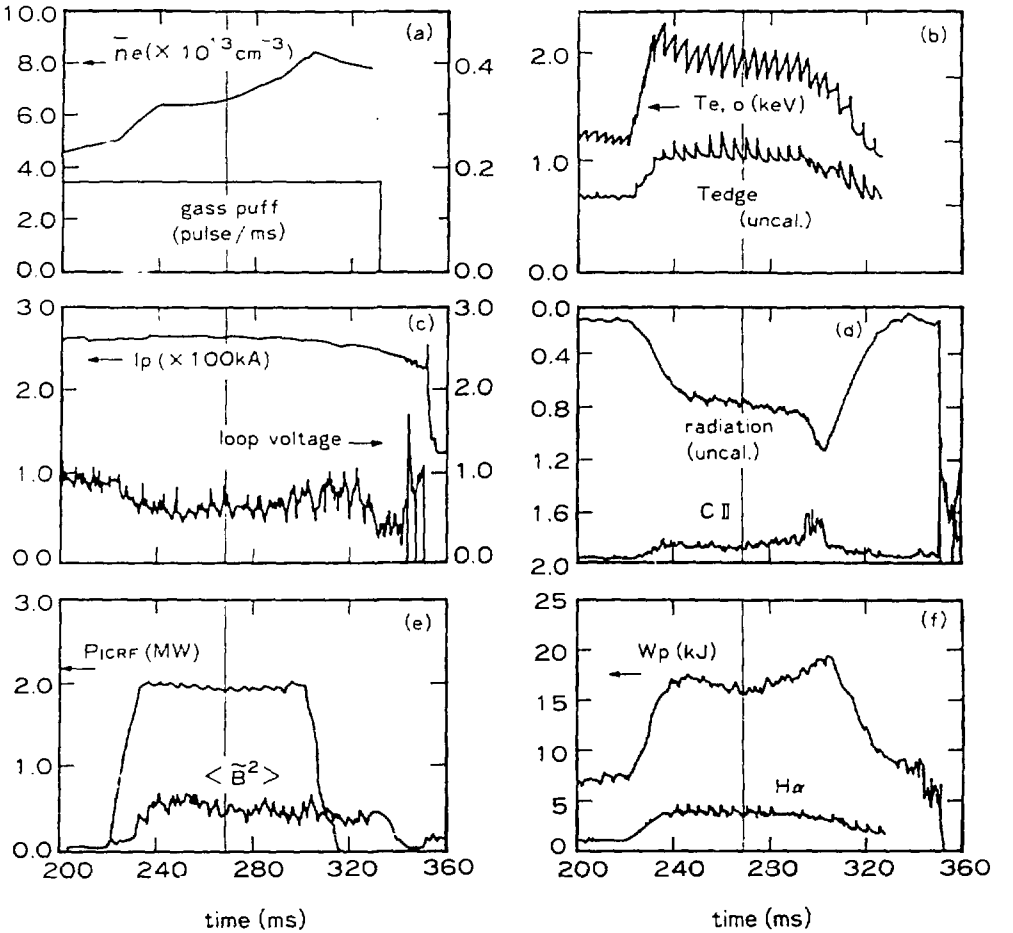
(a)
$\bar{n}e(\times 10^{13}cm^{-3})$
gass puff
(pulse / ms)
(b)
Te, o (keV)
Tedge
(uncal.)
(c)
Ip (×100kA)
loop voltage
(d)
radiation
(uncal.)
C II
(e)
PICRF (MW)
$<\tilde{B}^2>$
(f)
Wp (kJ)
Hα
time (ms)
time (ms)

Fig.16